The Decreasing Orbital Period of WASP-4b

L. G. BOUMA,[1] J. N. WINN,[1] T. DAYLAN,[2] K. G. STASSUN,[3, 4] S. KANE,[5] G. R. RICKER,[2] R. VANDERSPEK,[2] D. W. LATHAM,[6] S. SEAGER,[7] J. M. JENKINS,[8] TSO1,[8, 9] TSO2,[8, 9] TSO3,[8, 9] J. D. TWICKEN,[8, 9] B. WOHLER,[8, 9] D. A. CALDWELL,[8, 9] POC1, POC2, AND POC3

[1] *Department of Astrophysical Sciences, Princeton University, 4 Ivy Lane, Princeton, NJ 08540, USA*

[2] *Department of Physics and Kavli Institute for Astrophysics and Space Research, Massachusetts Institute of Technology, Cambridge, MA 02139, USA*

[3] *Vanderbilt University, Department of Physics & Astronomy, 6301 Stevenson Center Lane, Nashville, TN 37235, USA*

[4] *Fisk University, Department of Physics, 1000 17th Avenue N., Nashville, TN 37208, USA*

[5] *Department of Earth Sciences, University of California, Riverside, CA 92521, USA*

[6] *Harvard-Smithsonian Center for Astrophysics, 60 Garden Street, Cambridge, MA 02138, USA*

[7] *Department of Earth, Atmospheric, and Planetary Sciences, Massachusetts Institute of Technology, Cambridge, MA 02139, USA*

[8] *NASA Ames Research Center, Moffett Field, CA 94035, USA*

[9] *SETI Institute, Mountain View, CA, 94043*

ABSTRACT

Combining data from the Transiting Exoplanet Survey Satellite (TESS) with previous studies, we show that the transit times of WASP-4b are incompatible with a constant orbital period. In particular, the transits seem to have arrived 77.8 ± 10.7 seconds early, and the period appears to be shrinking by $\dot{P} = -12.1 \pm 1.2$ milliseconds per year. From TESS observations of WASP-6b, WASP-18b, and WASP-46b, we show that a systematic offset between the TESS time stamps and the barycentric reference sufficient to explain WASP-4b is ruled out at 6.3σ. If the timing variations are astrophysical, major contributors to the period change could include both apsidal precession and tidal decay. The Doppler shift from WASP-4's acceleration towards us could account for at most one quarter of the observed period change (at 2σ). Further transit and occultation studies will help confirm the reality of the timing variation, and eventually determine its cause.

1. INTRODUCTION

Long-term monitoring of hot Jupiter transit and occultation times should eventually reveal two distinct processes. First, whenever the summed spin and orbital angular momenta in a hot Jupiter system are below a particular critical value, the system will be unstable to tidal decay (Counselman 1973; Hut 1980). Most hot Jupiters satisfy this condition; their orbits should be shrinking (Levrard et al. 2009; Matsumura et al. 2010). The rate of decay is uncertain, and depends on how friction dissipates energy carried by gravitational tides (Ogilvie 2014 gives a review). If we could directly measure orbital decay rates, it would inform our understanding of tidal dissipation. This is important because the dissipation rates determine the fate of the system. During its inspiral, if the planet fills its Roche lobe below the stellar surface, the drag force from the stellar envelope accelerates the inspiral, leading to a 'direct-impact' merger (Metzger et al. 2012; MacLeod et al. 2018) Alternatively, if the planet fills its Roche lobe above above the stellar surface, then it could either be dynamically disrupted into an accretion disk or it could slowly transfer mass to the star (Metzger et al. 2012; Valsecchi et al. 2015; Jackson et al. 2016). Further afield, the outcome of the eventual interaction between the Earth and red giant Sun also hinges on the efficiency of tidal dissipation (Rasio et al. 1996).

The second process that long-term timing studies should reveal is rotation of the orbital ellipse within the orbital plane (apsidal precession). This effect has been studied extensively in eclipsing binaries (*e.g.*, Russell 1939; Schwarzschild 1958; Borkovits et al. 2015), and has been explored theoretically for transiting planets (Heyl & Gladman 2007; Pál & Kocsis 2008; Jordán & Bakos 2008; Ragozzine & Wolf 2009). However, apsidal precession has yet to be directly observed in hot Jupiters, and the orbits would need non-zero eccentricity for

Corresponding author: L. G. Bouma

luke@astro.princeton.edu

it to be detectable. Though the eccentricities of hot Jupiters are expected to be small, there are many mechanisms that could pump them away from circularity (see § 4.2, and Bailey & Goodman 2019). For hot Jupiters, the apsidal precession is usually dominated by the quadrupolar distortion of the planet by the star's tidal force (Ragozzine & Wolf 2009). If we measured apsidal precession in a hot Jupiter system, we could thus use the observed precession rate to compute the planet's Love number, giving a third parameter along with the mass and radius with which to describe the planet's interior structure (*e.g.*, Batygin et al. 2009, who performed a similar procedure for HAT-P-13b). Measuring small eccentricities and understanding their origin would also help us understand the dynamical histories and interior structures of hot Jupiters. (*e.g.*, Dawson & Johnson 2018; Ibgui et al. 2010, respectively)

While numerous indirect studies have called attention to population-level effects of tidal decay (Jackson et al. 2009; Hansen 2010; Penev et al. 2012; Husnoo et al. 2012; Matsakos & KÃŭnigl 2016; Collier Cameron & Jardine 2018; Penev et al. 2018), the most convincing direct evidence to date for either orbital decay or apsidal precession has come from WASP-12b. Maciejewski et al. (2016) showed that the transit times of WASP-12b did not follow a linear ephemeris at 5σ confidence, and measured $\dot{P} = -26 \pm 4\,\mathrm{ms\,yr^{-1}}$. Patra et al. (2017) presented new transit and occultation times for the system, and found $\dot{P} = -29 \pm 3\,\mathrm{ms\,yr^{-1}}$. Assuming that the period change was caused entirely by tidal decay, Patra et al. (2017) found values for the stellar quality factor of $Q'_\star \approx 2 \times 10^5$. This level of dissipation cannot be explained by standard equilibrium tide models (Penev & Sasselov 2011; Ogilvie 2014). Weinberg et al. (2017) found though that if WASP-12 were a subgiant, tidal dissipation due to a dynamical tide might be sufficient to produce the required level of friction. Bailey & Goodman (2019) concurred, but noted that the observational constraints on WASP-12 itself favor a main-sequence star, not a subgiant. More data are needed to determine the cause of the timing variations in WASP-12b.

This work focuses on WASP-4b, which is also a plausible candidate for orbital decay. The planet has radius $1.37 \pm 0.04\ R_{\mathrm{Jup}}$, and mass $1.29 \pm 0.10\ M_{\mathrm{Jup}}$ (Southworth 2011). It has an orbital period of 1.34 days, orbits its host star at a distance of $a/R_\star = 5.41$, and has been frequently observed over the past decade (Wilson et al. 2008; Huitson et al. 2017). The orbit is consistent with circular (Beerer et al. 2011; Husnoo et al. 2012; Bonomo et al. 2017, but see § 4.2). The host star is a G7V dwarf, with $R_\star = 0.92 \pm 0.13\ R_\odot$, $M_\star = 0.92 \pm 0.07\ M_\odot$, $T_{\mathrm{eff}} = 5400 \pm 90$ K, and an isochronal age of roughly 7 Gyr (Southworth 2011; Petrucci et al. 2013; Doyle et al. 2013).

We measure new transit times for WASP-4b using data from TESS (§ 2). We then merge these times with previous observations and compare three models for the times (§ 3): a constant period, a decaying period, and a slightly eccentric orbit undergoing precession. We rule out a constant period, but cannot firmly distinguish between the latter two possibil-
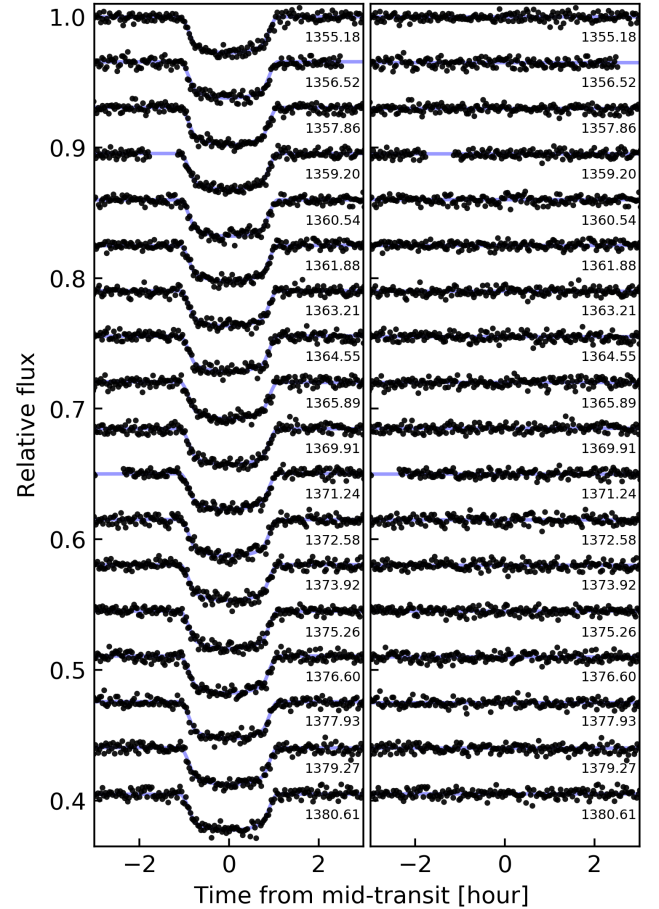
Figure 1. TESS transits of WASP-4b. On the left, black points are TESS flux measurements, with a vertical offset applied. Blue curves are best-fit models. Rounded midtimes are printed in BTJD next to the appropriate transits. The residuals are shown on the right.

ities. Each would have interesting implications (§ 4). We rule out the possibility that a systematic time system offset causes the observed variation (Appendix A), and conclude by advocating for further monitoring of the system (§ 5).

2. NEW TRANSIT TIMES

2.1. *Observations and cleaning*

WASP-4 was observed in TESS camera 2 from August 23, 2018 to September 20, during the spacecraft's second sector of science operations. The star is designated by the TESS Input Catalog as TIC 402026209 (Stassun et al. 2018).

The TESS spacecraft recorded images of WASP-4 in an 11×11 pixel array every 2 minutes. It was included on the "short-cadence" target list thanks to the Guest Investigator programs of J. Southworth and S. Kane (G011112 and G011183 respectively). After being downlinked through the Deep Space Network, the data were processed through the Science Processing Operations Center (SPOC) pipeline at NASA Ames (Jenkins et al. 2016). One important step in this processing was converting from spacecraft time to

barycentric time. SPOC then reports timestamps in "BTJD", where $BTJD = BJD - 2457000$, BJD is the barycentric julian date, and all times are in the TDB reference (see Urban & Seidelmann 2012 for explanations of time systems). The lightcurves were then vetted and released by the MIT TESS Science Office to the Mikulski Archive for Space Telescopes (Ricker & Vanderspek 2018).
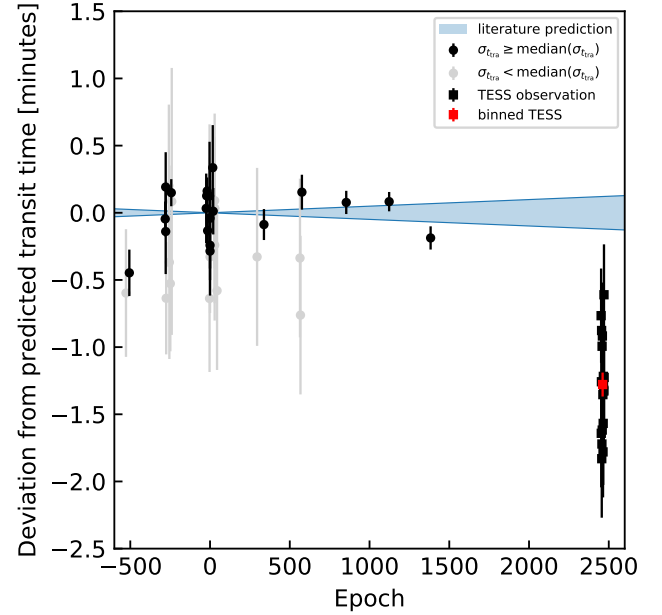
We begin our analysis with the Presearch Data Conditioning (PDC) light curves from MAST. The steps used to find an optimal aperture (for WASP-4, a 3×3 pixel array) and the PDC-MAP algorithm are described by Smith et al. (2017a) and Smith et al. (2017b) respectively.

We then processed the lightcurve as follows. First, we removed all points with non-zero quality flags. This removes data contaminated by coarse spacecraft pointing, cosmic rays, and other annoyances (Mansouri-Samani et al. 2018). We then filtered out known bad observing windows. The data closest to spacecraft perigee typically show ramp-like systematics, so we clipped out the first and last hour of both orbits. Next, we focused on the momentum dumps. As described in the data release notes[1], during the first two TESS sectors, every 2.5 days the spacecraft's reaction wheels were reset to maintain pointing stability. These events were assigned quality flags corresponding to "Reaction Wheel Desaturation Event" and "Manual Exclude". For WASP-4, these flags were simultaneously set for 54 distinct cadences, and there were 10 momentum dumps, averaging about 10 minutes of flagged data per dump. Simply out of caution, we clipped out an additional 10 minutes before and after every momentum dump. Before applying any filters, we had 19737 data points. After applying all the filters, we were left with 18165 measurements, or 92% of the original data.

After "cleaning" the data, we normalized the flux measurements by dividing out the median flux. We then converted the timestamps from BTJD to BJD by adding the appropriate 2457000 day offset (Mansouri-Samani et al. 2018). Many of these and subsequent processing steps were performed using `astrobase` (Bhatti et al. 2018) We opted not to "flatten" the lightcurves at this stage, as is often done with *e.g.*, a spline or gaussian process regression. Such procedures are asymmetric about the transit minimum and can skew the transit time measurement without being captured by the measurement uncertainties.

2.2. *Measuring the transit times*

Using the times, flux measurements, and errors determined above, we ran Box Least Squares (BLS) to estimate the transit epoch, period, and duration (Kovács et al. 2002). From the BLS parameters, we isolated each transit to within ± 10 transit durations of its midtime. In each transit window, we then simultaneously fit for a model transit, plus a local linear trend. Our transit model uses the analytic formulae calcu-

lated by Mandel & Agol (2002) and implemented by Kreidberg (2015).

We allowed four free parameters per transit: the time of mid-transit t_{tra}, the planet-to-star radius ratio $R_p/R_\star$, and the slope and intercept of the line. We fixed the remaining transit parameters as follows. We set the eccentricity to zero, and the longitude of periastron to $\pi/2$. We assumed a quadratic limb-darkening law, with coefficients interpolated from the Claret (2017) tables. For the period, $a/R_\star$, and inclination, we adopted the values from Petrucci et al. (2013). These are in reasonable agreement with the parameters reported by Gillon et al. (2009b), Southworth et al. (2009), and Huitson et al. (2017).

Having defined the free and fixed parameters, we calculated an initial guess for the free parameters by maximizing the likelihood. We then sampled over the posterior using the algorithm proposed by Goodman & Weare (2010) and implemented by Foreman-Mackey et al. (2013). During this process, we used the `corner` software to check that our posteriors were being well-sampled (Foreman-Mackey 2016).

After performing the initial fit, we set the photometric error bars to be equal to the standard deviation of the in-transit points of the residual lightcurve. We then reperformed the same fitting procedure, using the empirically determined photometric errors.

Figure 2. TESS saw WASP-4b transit earlier than expected. Points are differences between observed transit times and the constant-period ephemeris we fit to literature transits. Black points are the more precise half of literatures times; gray points are the less precise half. The blue curves represent the $\pm 1\sigma$ credible interval around the constant-period ephemeris. The binned TESS observation (red point) arrived 77.8 ± 10.7 seconds before it was expected.

---

[1] archive.stsci.edu/hlsps/tess-data-alerts/hlsp_tess-data-alerts_tess_phot_s01_tess_v1_release-notes.pdf

To check that the measured uncertainties are plausible, we computed the reduced χ^2 for a linear ephemeris fit to the measured TESS transit times. We found that $\chi^2 = 8.4$, with 16 degrees of freedom. Examining the residuals by eye showed that the error variance was being overestimated, so we multiplied the measured TESS errors by a factor $f = 0.73$, forcing a reduced χ^2 of unity. This reduced the mean transit time uncertainty from $\sim$30 seconds per transit to $\sim$22 seconds per transit.

Figure 1 shows the light curves, best-fit transit models, and residuals. Table 1 reports the mid-transit times and their uncertainties, and also includes the previously reported times analyzed in § 3.

Taking the mean and standard deviation of the measured planet to star radius ratio, we find $R_\mathrm{p}/R_\star = 0.1538 \pm 0.0013$, in agreement with previous determinations (Wilson et al. 2008; Gillon et al. 2009b; Winn et al. 2009; Southworth et al. 2009).

Binning the residuals to 1-hour windows and taking the median absolute deviation, we measure a MAD of the residual lightcurves of 594 ppm hr$^{1/2}$. WASP-4 has a TESS-band magnitude of $T = 11.78$ (Stassun et al. 2018), corresponding to a predicted photon-counting noise[2] of 410 ppm hr$^{1/2}$. At $T = 11.78$, with a 9-pixel aperture read noise is expected to contribute an additional 202 ppm hr$^{1/2}$ in quadrature. The predicted zodiacal background contribution is 673 ppm hr$^{1/2}$, based on the Winn (2013) model, which was used in the Sullivan et al. (2015) planet detection simulations. The predicted level of zodiacal noise seems to have been an overestimate, given the observed RMS of WASP-4. A more detailed assessment of TESS's photometric performance is beyond the scope of this work.

3. TIMING ANALYSIS

3.1. *Times*

Table 1 shows all the transit times used in our analysis. We included data from peer-reviewed literature for which the analysis was based on observations of a single, complete transit, and for which the midpoint was fit as a free parameter. We also required that the time system be clearly documented.

Table 2 shows the occultation times. Since there are fewer available, we included all the occultation measurements we could find. The tabulated values have been corrected for the light-travel time across the diameter of the orbit by subtracting $2a/c = 22.8$ seconds from the observed time.

We use the homogeneous Hoyer et al. (2013) timing study as our starting point. We took their BJD$_\mathrm{TT}$ times to be equivalent to times in BJD$_\mathrm{TDB}$, since the two time systems differ periodically by only milliseconds (Urban & Seidelmann 2012). We verified that their times, as well as all others, were on the BJD$_\mathrm{TDB}$ time standard using the calculator provided by Eastman et al. (2010). We set the zero-point epoch to be as close as possible to the average of the transit times, weighted as

the inverse midtime variance. This minimizes the covariance between the transit epoch and the period (Gibson et al. 2013).

Important contributions to the timing dataset are as follows. The earliest epoch in our fit is from the EulerCam lightcurve observed by Wilson et al. (2008). The second, more precise, epoch comes from z-band photometry acquired by Gillon et al. (2009b) at the VLT with FORS2. Subsequent epochs came from Winn et al. (2009)[3], Dragomir et al. (2011), Sanchis-Ojeda et al. (2011), and Nikolov et al. (2012). Hoyer et al. (2013) reported nine transit observations taken with the the Y4KCAM on the SMARTS 1-m telescope, and another three with the SOI on the SOAR 4.2-m telescope. Hoyer et al. (2013) also homogeneously redetermined the transit times from all previous studies. Though their latest two epochs fell slightly below the prediction of a linear ephemeris (Panel C of their Figure 6), they did not find a need to fit a quadratic function to the O-C values.

After the study by Hoyer et al. (2013), Ranjan et al. (2014) acquired near-IR spectra of WASP-4b using HST's WFC3 in both transit and secondary eclipse. We adopt only their transit time, since the epoch of occultation was not fit as a free parameter. Huitson et al. (2017) acquired optical transmission spectra with the 8.1-m Gemini South telescope over 2011 to 2014, one transit per season. The per-point standard deviation of their lightcurves is a few hundred parts per million, less than a factor of 3 away from the photon noise limit. The uncertainties on their reported transit times – on average 5.6 seconds – are small, but possible given the quality of their data (cf. Carter et al. 2008).

There have been other studies of WASP-4b for which the transit timing data are either hetereogenous, not available, or not useable. We omitted the timing measurements from Southworth et al. (2009), since there were technical problems with the computer clock at the time of observation (Nikolov et al. 2012). The timing study by Petrucci et al. (2013) ruled out transit timing variations larger than 54 seconds over the previous 5 years, but did not report transit times. Baluev et al. (2015) collected transit times for many hot Jupiters, including WASP-4b, and included times from the Exoplanet Transit Database (ETD)[4] (Poddaný et al. 2010). Since the ETD data come from heterogeneous sources, their timestamps are less clearly documented, and the times are thus more prone to systematic errors, we omit them from consideration. May et al. (2018) obtained optical spectra using IMCAS on Magellan, and found a flat transmission spectrum, in agreement with the results reported by Huitson et al. (2017). They did not report transit times.

There are fewer available occultation times. Beerer et al. (2011) observed two occultations of WASP-4b using warm Spitzer in the 3.6 μm and 4.5 μm bands. Cáceres et al. (2011) detected an occultation from the ground in the K$_\mathrm{s}$ band, and gave a time in HJD, without specifying the time standard.

---

[2] github.com/lgbouma/tnm

[3] Winn et al. (2009) recorded the GPS clock time in UT reference. They then converted this to BJD in the TDB reference for their reported midtimes.

[4] http://var2.astro.cz/ETD/
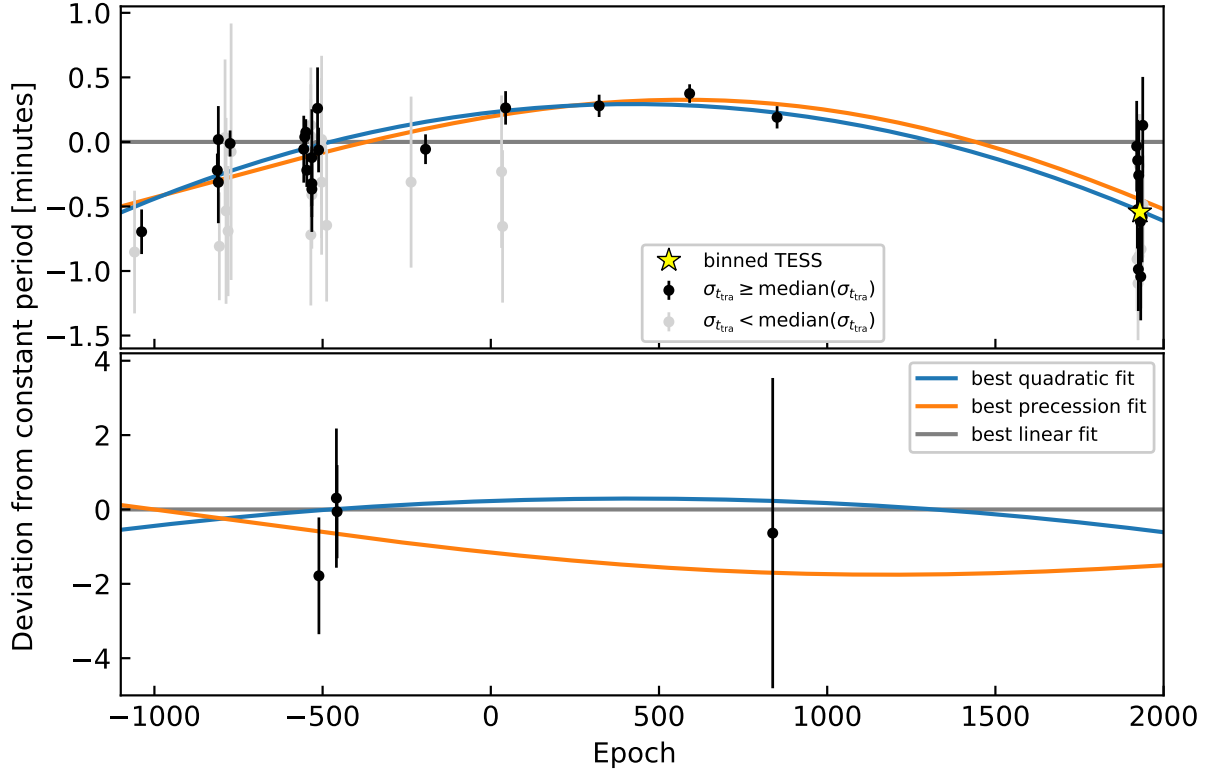
Figure 3. Timing residuals and best-fit models for WASP-4b. Points are differences between observed transit times and a linear ephemeris fit to all the times. The constant period model is a poor fit to the observed times (gray line). Black points are the more precise half of measured times; gray points are the less precise half. The blue curve is the best-fit model with a constant period derivative. The orange curve is the best-fit model assuming apsidal precession causes the observed timing deviations.

We correspondingly added 69.184 seconds of uncertainty to their reported errors, in quadrature. Finally, as previously mentioned, Ranjan et al. (2014) acquired occultation data with HST but kept the epoch as a fixed parameter. Zhou et al. (2015) performed a similar analysis with occultation data from the Anglo-Australian Telescope, focusing on the eclipse depth, but also fitting for $e\cos\omega$. We converted their $e\cos\omega$ results into a midtime, using their ephemeris and the standard formula (*e.g.*, Charbonneau et al. 2005; Winn 2010)

$$t_{\text{occ}}(E) = t_0 + PE + \frac{P}{2}\left(1 + \frac{4}{\pi}e\cos\omega\right). \quad (1)$$

This gives us a total of 4 occultations. Although their timing error bars are large compared to the transits, we include them for completeness, and because they can help in our modeling of the timing variations.

3.2. *Analysis*

After collecting the literature times and measuring the TESS times, we compared the observed time to the prediction based solely on the literature times. The result is shown in Figure 2. The TESS observations appear to have arrived early. One immediate concern was systematic errors in either the archival or the TESS timestamps. The tests we used to mitigate the latter possibility are described in Appendix A.

Assuming that the observed timing variation is astrophysical, we proceeded by exploring three models for the timing data, identical to the study by Patra et al. (2017).

The first model assumes a constant orbital period on a circular orbit:

$$t_{\text{tra}}(E) = t_0 + PE, \quad (2)$$

$$t_{\text{occ}}(E) = t_0 + \frac{P}{2} + PE, \quad (3)$$

for E the epoch number. The two free parameters are the reference epoch t_0 and the period P.

The second model assumes a constant period derivative, and a circular orbit:

$$t_{\text{tra}}(E) = t_0 + PE + \frac{1}{2}\frac{dP}{dE}E^2, \quad (4)$$

$$t_{\text{occ}}(E) = t_0 + \frac{P}{2} + PE + \frac{1}{2}\frac{dP}{dE}E^2. \quad (5)$$

The three free parameters are the epoch, period at the reference epoch, and period derivative, $dP/dt = (1/P)dP/dE$.

The third model assumes the planet has a slightly eccentric orbit, and that the line of apsides is rotating:

$$t_{\text{tra}}(E) = t_0 + P_s E - \frac{eP_a}{\pi}\cos\omega, \qquad (6)$$

$$t_{\text{occ}}(E) = t_0 + \frac{P_a}{2} + P_s E + \frac{eP_a}{\pi}\cos\omega, \qquad (7)$$

for P_s the sidereal period, e the eccentricity, P_a the anomalistic period, and ω the argument of pericenter. Following Giménez & Bastero (1995) and Patra et al. (2017), in this model the angular velocity of the line of apsides $d\omega/dE$ is constant,

$$\omega(E) = \omega_0 + \frac{d\omega}{dE}E, \qquad (8)$$

and the sidereal and anomalistic periods are related by

$$P_s = P_a\left(1 - \frac{1}{2\pi}\frac{d\omega}{dE}\right). \qquad (9)$$

The five free parameters are the epoch, sidereal period, eccentricity, argument of pericenter at the reference epoch, and angular velocity of line of apsides: $(t_0, P_s, e, \omega_0, d\omega/dE)$.

Assuming the error bars on the transit midtimes are gaussian and independent, we then proceed by fitting each model to the timing data. For the linear model, we took uniform priors over small windows around the expected parameters. For the quadratic model we did the same, and took the quadratic term to have a uniform prior corresponding to $Q'_\star \sim \mathcal{U}[10^3, 10^9]$, for $Q'_\star$ the modified quality factor defined in § 4. For the precession model, we took the same priors in epoch and sidereal period, and drew the remaining parameters from wide uniform distributions.

Figure 3 shows the residuals with respect to the linear model. The median MCMC linear fit has $\chi^2 = 149$ and 58 degrees of freedom. The median MCMC quadratic fit has $\chi^2 = 48.0$ and 57 degrees of freedom. The median MCMC precession fit has $\chi^2 = 51.0$ and 55 degrees of freedom.

The difference in χ^2 between the linear and quadratic fit corresponds to $p \approx 10^{-23}$. In other words, assuming the linear model is true, there is a 10^{-23} probability that simply by chance we would see data that favors the quadratic model more strongly than the observations. A more likely possibility is some systematic error being present in one of the most important sets of times: either the earliest times, the Huitson et al. Gemini times (epoch numbers 44, 322, 591, and 851), or the TESS times. We have taken every precaution against systematic offsets in the TESS dataset (Appendix A), and Huitson et al. stand by their reported times (Huitson, priv. comm.). Since the linear model provides a poor fit to the data, we discard it from further consideration.

The quadratic model fits better than the precession model. It is favored over the precession fit by $\Delta\chi^2 = 3.0$, and has two fewer free parameters. Another useful heuristic for model comparison is the Bayesian Information Criterion (BIC),

$$\text{BIC} = \chi^2 + k\log n, \qquad (10)$$

for k the number of free parameters, and n the number of data points. For us, $n = 60$. The difference in the BIC for the precession and decay models is $\Delta\text{BIC} = \text{BIC}_{\text{prec}} - \text{BIC}_{\text{quad}} = 11$, corrsonding to a Bayes factor of $\approx 4 \times 10^4$. In the language of Kass & Raftery (1995), this is "decisive evidence" for the quadratic model describing the data better than the precession model. Using the Akaike Information Criterion similarly favors the orbital decay model, by $\Delta\text{AIC} = 7$.

Assuming the orbital decay model, we find a period derivative

$$\dot{P} = -(3.82^{+0.38}_{-0.37}) \times 10^{-10} = -(12.1^{+1.2}_{-1.2})\,\text{ms yr}^{-1}. \qquad (11)$$

For comparison, the period derivative seen by Maciejewski et al. (2016) and Patra et al. (2017) in WASP-12b is $\dot{P} = -29 \pm 3\,\text{ms yr}^{-1}$. Assuming the quadratic model, WASP-4b is thus decaying at about half the rate as WASP-12b.

If we instead assume the precession model, the best-fit eccentricity is $e = (1.63^{+1.48}_{-0.65}) \times 10^{-3}$. The longitude of periapse correspondingly advances by $\dot{\omega} = 14.8^{+5.4}_{-3.8}$ degrees yr^{-1}. The corresponding precession period would be 24^{+8}_{-6} years.

The median parameters and their standard deviations are reported for all the models in Table 3. To summarize, a linear ephemeris does not describe the observed times. Both orbital decay and precession can fit the observed data. However, the precession model has two extra free parameters, and is statistically disfavored. Further observations will help discriminate between orbital decay and precession.

4. IMPLICATIONS

4.1. *Orbital decay*

The middle panel of Figure 4 shows the expected orbital decay time of WASP-4b compared to other transiting giant planets. Though there are roughly 20 hot Jupiters that might be expected to decay faster, some orbit stars with minimal convective zones (*e.g.*, WASP-18), and most are not as well-observed as WASP-4.

Let us assume for the sake of argument that the observed timing variation is caused entirely by orbital decay. If the period decreases at a fixed rate, it will reach zero after

$$\frac{P}{\dot{P}} = 9.6\,\text{Myr}. \qquad (12)$$

For comparison, the "survival time" found by Patra et al. (2017) for WASP-12b was 3.2 Myr.

Let us assume further that the "constant phase lag" model for tidal interaction in a binary applies (Zahn 1977). The fluid response is parametrized by a constant modified[5] quality factor, $Q'_\star = 3Q_\star/(2k_\star)$. Here $k_\star$ is the stellar Love number, which is smaller when the star's density distribution is more centrally concentrated. $Q_\star$ is the ratio of the energy stored in the equilibrium deformation of the star, divided by the energy dissipated per tidal period (*e.g.*, Goldreich & Soter

---

[5] For stars, $k_\star \sim \mathcal{O}(10^{-2})$, so it is important to explicitly distinguish $Q'_\star$ from $Q_\star$ (*e.g.*, Schwarzschild 1958).
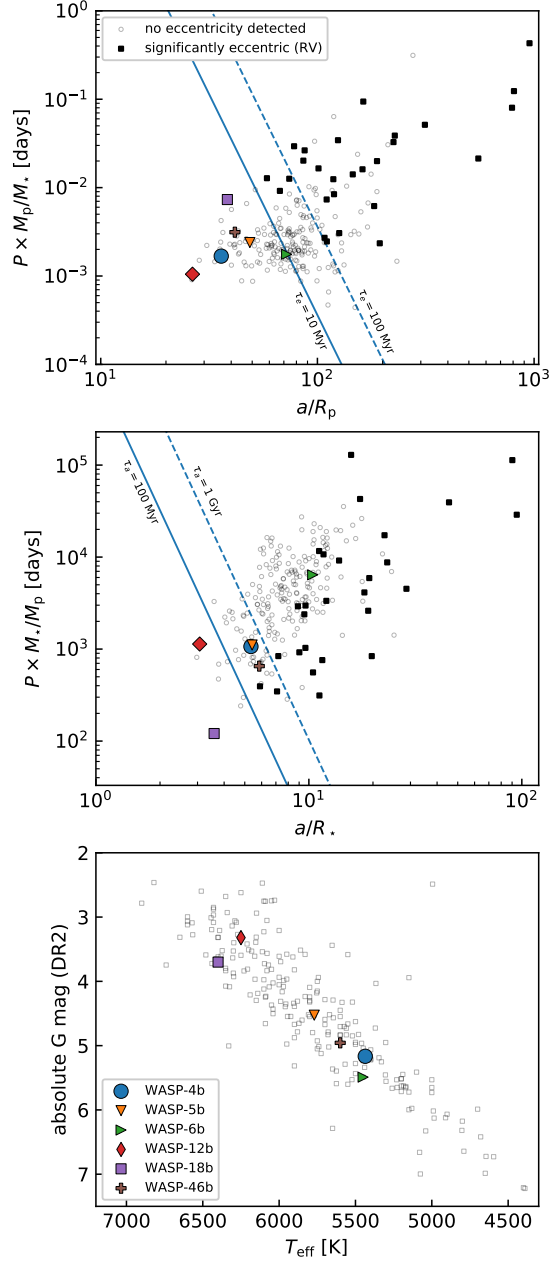
Figure 4. WASP-4b has a short eccentricity damping time and medium decay time compared to other hot Jupiters. It seems to orbit a main sequence host. *Top:* Transiting giant planets from Bonomo et al. (2017), who measured the eccentricities using radial velocities. Solid squares (including WASP-18b) have significant eccentricity detections. The axes are chosen so that constant eccentricity damping timescales (Equation 13) are lines. The contours shown assume $Q'_p = 10^5$. *Middle:* Axes are chosen so to that constant orbital decay timescales (Equation 14) are lines. The contours shown assume $Q'_\star = 10^7$. *Bottom:* HR diagram highlighting WASP-12b, which shows timing variations similar to WASP-4b. We also show hot Jupiters for which we detect no timing variation (see § A.2).

1966). A larger $Q_\star$ implies less efficient dissipiation. Though

the fluid mechanics responsible for the dissipation should depend on the amplitude and frequency of the tidal perturbation (Ogilvie 2014, Section 3.3), we will treat $Q'_\star$ as a constant. This should not be taken literally; $Q'_\star$ may in fact change sharply with varying tidal frequency (Penev et al. 2018).

If the planet's spin and orbit are synchronized, the star is slowly rotating, and the eccentricity is small, then the semimajor axis and eccentricity evolve as (Metzger et al. 2012, Appendix B)

$$\frac{1}{\tau_e} = \frac{|\dot{e}|}{e} = \frac{63\pi}{2Q'_p}\left(\frac{R_p}{a}\right)^5\left(\frac{M_\star}{M_p}\right)\left(\frac{1}{P}\right) \tag{13}$$

$$\frac{1}{\tau_a} = \frac{|\dot{a}|}{a} = \frac{9\pi}{Q'_\star}\left(\frac{R_\star}{a}\right)^5\left(\frac{M_p}{M_\star}\right)\left(\frac{1}{P}\right). \tag{14}$$

The orbital period evolves as

$$\dot{P} = -\frac{27\pi}{2Q'_\star}\left(\frac{M_p}{M_\star}\right)\left(\frac{R_\star}{a}\right)^5. \tag{15}$$

Inserting our observed value of $\dot{P}$, the current dissipation rate corresponds to a modified quality factor for WASP-4 of

$$Q'_\star \approx 3.3 \times 10^4. \tag{16}$$

This is rather small. Jupiter has $Q'_{Jup} \approx 1.4 \times 10^5$, based on the motion of the Galilean moons (Lainey et al. 2009). For stars, different $Q'_\star$ values have been estimated in different contexts. Studies of the observed eccentricity distribution in stellar binaries have yielded $10^5 \gtrsim Q'_\star \gtrsim 10^7$ (*e.g.*, Meibom & Mathieu 2005; Belczynski et al. 2008; Geller et al. 2013; Milliman et al. 2014). However the dissipation rates may be different in hot Jupiter systems, since the tidal forcing frequencies and amplitudes are different. In fact, for the observed population of hot Jupiters, Penev et al. (2012) argued that $Q'_\star > 10^7$ would be required at some phase of hot Jupiter evolution at the 99% level, or else the observed population would not exist (though Birkby et al. 2014 point out more efficient dissipation would be allowed if the hot Jupiters arrived later). Developing a generative model for the orbital separation distribution of the hot Jupiter population, Collier Cameron & Jardine (2018) similarly found $10^7 \gtrsim Q'_\star \gtrsim 10^8$.

Using an empirical approach, Penev et al. (2018) reported a $Q'_\star$ measurement for WASP-4. In earlier work, Penev et al. (2016) noted that HATS-18b and WASP-19b orbited host stars whose isochronal ages are consistent with the Sun, but whose stellar rotation periods are about 10 days (Pont 2009 pointed out similar evidence for hot Jupiter host spin-up). The expected rotation periods at solar ages are 20 to 30 days (Schatzman 1962; Skumanich 1972, and measurements by Barnes et al. 2016 in the 4 Gyr-old M67 cluster). Assuming that the difference between the observed and predicted stellar rotation period was due to tides depositing angular momentum in the star, Penev et al. (2018) modeled the evolution of hot Jupiter systems under the influence of a magnetized wind and a constant phase-lag tide. They found two-sided limits for $Q'_\star$ in 35 of the 188 systems they examined. In these 35

systems, they found that $Q'_\star$ varied from 10^5 at tidal periods of 2 days to 10^7 at tidal periods of 0.5 days. For WASP-4 specifically, their method gave $Q'_\star \approx (1.2^{+1.0}_{-0.5}) \times 10^7$. This is more than 2 orders of magnitude less efficient than the dissipation rate inferred from the decaying orbit would imply.

A different model for tidal dissipation was discussed by Essick & Weinberg (2016), who considered the nonlinear response of the star to a coupled network of gravity modes excited at the base of the convective zone, and braking near the stellar core. In their approach, the stellar tidal quality factors in hot Jupiter systems vary from $Q'_\star \approx 10^5 - 10^6$. Using their Equation 26, the prediction for WASP-4 is that it has $Q'_\star = 7 \times 10^5$. This is one order of magnitude larger than would be implied by the observed period change.

The applicability of the Essick & Weinberg (2016) model depends on the evolutionary state of the star. The bottom panel of Figure 4 shows WASP-4 in the context of other giant planet hosts from the Bonomo et al. (2017) sample. On the y-axis is $G = g - \mu$, for g the apparent Gaia-band magnitude, and μ the distance modulus reported by Gaia Collaboration et al. (2018). The x-axis is the effective temperature from Bonomo et al. (2017), which for WASP-4 agrees within 1σ of that reported by Petrucci et al. (2013). By visual inspection of the HR diagram, WASP-4 shows litle evidence of being evolved. By a similar argument though, WASP-12 would not clearly stand out as a candidate subgiant, and Weinberg et al. (2017) suggest it may in fact be a subgiant (though Bailey & Goodman 2019 do not find evidence that supports this suggestion). A more thorough isochronal analysis would be of interest, particularly if the transit and occultation times continue to vary. Such an analysis is beyond the scope of this study.

In short, if the observed period change is caused entirely by tidal decay, it would imply a tidal dissipation efficiency stronger than typical orbit-averaged predictions. It might be possible that we are observing at a special time, when the planet is near resonance with the some stellar oscillation mode, and the energy dissipation is exceptionally large (Ogilvie 2014; Essick & Weinberg 2016). Tidal dissipation rates might also be increased if the star is turning off the main sequence. WASP-4 shows little evidence for this; it is unclear that tidal decay could explain its changing period.

4.2. Apsidal precession

Let us instead assume that the entire timing variation can be explained as being a portion of an apsidal precession cycle. The required orbital eccentricity is then

$$e = (1.6^{+1.5}_{-0.7}) \times 10^{-3}, \tag{17}$$

and the line of apsides is advancing by

$$\dot{\omega} = 14.8^{+5.4}_{-3.8} \ \text{degrees yr}^{-1}. \tag{18}$$

One full precession period would take about 24 years, or twice the current observing baseline.

Ragozzine & Wolf (2009) calculated apsidal precession periods for hot Jupiters ranging between of order 10 and 100

years. They highlighted that for many hot Jupiters, including WASP-4b, over 90% of the apsidal precession comes from the tidal bulge of the planet. Precession from general relativity, the planet's rotational bulge, and the star's rotational and tidal bulges are minor contributors. Ragozzine & Wolf (2009) also calcuated that WASP-4b was expected to have a relatively short precession period, of 120 years.

Ragozzine & Wolf (2009) also noted that if the planet has non-zero eccentricity, a measurement of $\dot{\omega}$ can be converted into a measurement of the planetary Love number, $k_{2,p}$. From Ragozzine & Wolf (2009) Equation 14, the implied planetary Love number for WASP-4b is

$$k_{2,p} = 1.6^{+2.1}_{-1.2}. \tag{19}$$

For comparison, $k_{2,\text{Jup}} \approx 0.59$ (Wahl et al. 2016, bug see Ni 2018). A uniform density sphere has $k_2 = 1.5$. Our reported uncertainties on $k_{2,p}$ are large because the eccentricity, reference time, and $d\omega/dE$ are quite correlated, and the measured occultation times only barely constrain them (Figure 5).

4.2.1. Empirical constraints on small eccentricities in hot Jupiters

Could the eccentricity truly be non-zero? For WASP-4b, the eccentricity damping timescale (Equation 13) is $\tau_e = 0.29(Q'_p/10^5)\,\text{Myr}$. The system appears to be well over $1\,\text{Gyr}$ old (Winn et al. 2009), so any initial eccentricity should have been erased.

The top panel of Figure 4 compares the expected eccentricity damping time of WASP-4b with other transiting giant planets. WASP-4b has one of the shortest known eccentricity damping times. The hot Jupiter with the nearest τ_e and a significant measured eccentricity is WASP-18b, with $e = 0.0076 \pm 0.0010$ (Triaud et al. 2010; Bonomo et al. 2017). This is the smallest significant eccentricity measured by the RV method, with the next-smallest cases being HAT-P-20b ($e = 0.01580^{+0.0023}_{-0.0018}$), and WASP-38b ($e = 0.02780^{+0.003}_{-0.0028}$). For the 231 planets studied by Bonomo et al. (2017), 2 (13) had 2σ upper limits of $e < 0.01$ ($e < 0.02$). For WASP-4b, the strongest 2σ upper-limit on its eccentricity from RVs is $e < 0.011$ (Husnoo et al. 2012; Bonomo et al. 2017).

Occultation timing can provide stronger eccentricity limits than RV measurements, but they often come with caveats. For WASP-4b, the strongest limit on its eccentricity comes from Beerer et al. (2011), who observed occultations and derived a 2σ upper limit on $|e\cos\omega|$ of 0.0024. Placing eccentricity limits stronger than $e < 10^{-3}$ has only been possible for a few hot Jupiters, and with numerous false-starts. HD 189733b, for example, was initially reported to have a non-zero eccentricty, $e\cos\omega = 0.0010 \pm 0.0002$ (Knutson et al. 2007). This result was retracted by Agol et al. (2010), who used a larger dataset of 7 Spitzer eclipses and found a smaller average offset in the secondary eclipse time than Knutson et al. (2007). Agol et al. (2010) also noted that a larger fraction of the planet's observed occultation time offset could be explained by detailed modeling of the planetary hot-spot, which can shift occultation times by up to a few minutes (Williams et al. 2006). Including an updated hot-spot model,

Agol et al. (2010) reported a 2σ limit of $e\cos\omega < 0.00023$, perhaps the strongest eccentricity limit yet for a hot Jupiter. A similar saga occurred for HD 209458b, for which Winn et al. (2005) combined Spitzer secondary eclipses with RV data and reported a small finite eccentricity. They suspected that the data were consistent with zero eccentricity, and that the lower bound on e was an artifact of an imperfect limb-darkening model. Crossfield et al. (2012) eventually found stronger limited: $e\cos\omega < 0.0007$ at 2σ. The final example is WASP-12b, for which the discovery RVs and photometry gave a small finite eccentricity measurement (Hebb et al. 2009, at 3σ). A prompt ground-based occultation measurement by López-Morales et al. (2010) concurred that a small eccentricity was favored with weak statistical significance. Further follow-up found occultation times consistent with circular orbits; $|e\cos\omega| < 0.0040$ (Campo et al. 2011; Croll et al. 2011).

In summary, empirical constraints on the ellipticity of hot Jupiter orbits at the $e \lesssim 10^{-3}$ level are present only for HD 189733b and HD 209458b, from occultation timing. Once the timing offsets are of order tens of seconds, eccentricities from occultation timing may have systematic uncertainties because of the hot-spot issue (Williams et al. 2006; Agol et al. 2010). With the exception of WASP-18b, radial velocity measurements have provided eccentricity constraints only at the $e > 10^{-2}$ level. Empirical cannot rule out hot Jupiter eccentricities at the level needed to contextualize WASP-4.

4.2.2. *Theoretical expectations for small eccentricities in hot Jupiters*

Lacking empirical data, we now turn to theoretical mechanisms that could produce small eccentricities.

Neighboring companion—Mardling (2007) considered the long-term tidal evolution of hot Jupiters with companions. They pointed out that although the early phases of the two-planet eccentricity evolution would occur quickly, the final phase of the joint eccentricity evolution towards circularity would often occur on timescales several orders of magnitude longer than the circularization time (see their Figures 4 and 5). The companion in their model is coplanar, and can have a mass down to an Earth-mass; the main requirement is that both the hot Jupiter and the outer companion start on eccentric orbits.

Another mechanism to excite the hot Jupiter's eccentricity is the Kozai-Lidov mechanism (Lidov 1962; Kozai 1962). In this case, the orbital plane of the outer companion, "c", would need to be inclined relative to that of the hot Jupiter, "b", by at least $\sin^{-1}\sqrt{2/5} \approx 39°$. Bailey & Goodman (2019) point out how the joint requirements of Kozai-Lidov oscillations with a non-detection of an additional RV signal can be combined to produce lower and upper limits on the companion's mass. For the Kozai-Lidov mechanism to operate, from Bailey & Goodman (2019) Equation 20 we need

$$M_{\rm c} > 7.7\,M_{\oplus} \times \left(\frac{a_{\rm c}}{a_{\rm b}}\right)^{3/2}, \qquad (20)$$

where $M_{\rm b,c}$ and $a_{\rm b,c}$ are the mass and semi-major axis of WASP-4b and the hypothetical WASP-4c, and we have assumed WASP-4b's Love number is $k_{2,\rm b} \approx 0.6$. For the RV signal of the companion to remain undetected, it would need to be in the residual $(\rm O-C)_{\rm RV} = 15.2\,{\rm ms}^{-1}$ reported by Triaud et al. (2010). Again following Bailey & Goodman (2019), this implies

$$M_{\rm c} < (\rm O-C)_{\rm RV} \left(\frac{M_{\star}a_b}{G}\right)^{1/2} \left(\frac{a_c}{a_b}\right)^{1/2} f^{-1/2}$$

$$M_{\rm c} < 24.2\,M_{\oplus} \times \left(\frac{a_c}{a_b}\right)^{1/2} f^{-1/2}, \qquad (21)$$

for $f(e_{\rm c},\omega_{\rm c},i_{\rm c}) \propto \sin^2 i_{\rm c}$ a geometric prefactor that depends on the argument of periastron $\omega_{\rm c}$ and inclination $i_{\rm c}$ of the exterior companion (Bailey & Goodman 2019 Equation 23). Since WASP-4b transits along the line of sight, f can be arbitrarily small, and both of the preceding limits can be easily satisfied. This mechanism could produce the needed eccentricity. However it would be more satifying if long-term radial velocity monitoring showed an additional planet in the system. The chances of one existing with a mass between 1-13 $M_{\rm Jup}$ and orbital semi-major axis between 1-20 AU is about 50%, and a linear trend is currently present at $\sim 2\sigma$ (Knutson et al. 2014).

Fluctuations in the gravitational potential from convection—A separate mechanism that might produce the eccentricity is simply stellar convection (Phinney 1992, Section 7). Phinney presents this idea by analogy with a pendulum, which is never really at rest. Instead, collisions with air molecules randomly perturb its momentum and energy, and the equipartition theorem of statistical mechanics tells us the average energy is $\langle E_{\rm pend}\rangle = kT_{\rm air}$. In hot Jupiter systems, the "air molecules" are convective eddies, and their associated kinetic energy leads the orbit to never have exactly zero eccentricity. In particular, from Phinney 1992 Equation 7.33,

$$\langle e^2\rangle = \frac{2\langle E_{\rm e}\rangle}{\mu n^2 a^2} = 6.8 \times 10^{-5} \frac{(L^2 R_{\rm conv}^2 M_{\rm conv}^2)^{1/3}}{\mu n^2 a^2}, \qquad (22)$$

for L the stellar luminosity, $R_{\rm conv}$ ($M_{\rm conv}$) the width (mass) of the convective region, μ the reduced mass, n the orbital frequency, and a the semi-major axis. For WASP-4, convection in the star is more important than convection in the planet, and $\langle e^2\rangle^{1/2} < 10^{-5}$.

4.3. *Applegate effect*

Some eclipsing binaries exhibit period modulations with amplitudes of $\lesssim 0.05$ days over timescales of decades (*e.g.*, Söderhjelm 1980; Hall 1989). Applegate (1992) proposed a mechanism to explain these modulations in which the internal structure of a magnetically active star changes shape via cyclic exchange of angular momentum between the inner and outer zones of the star. This model could also apply to a hot Jupiter orbiting a star with a convective zone. The changing gravitational quadrupole of the star would cause the orbit of

the planet to precess on the timescale of the stellar activity cycle ("the dynamo timescale"). An essential difference between this process and apsidal precession is that it is expected to be quasi-periodic (*e.g.*, Söderhjelm 1980, Figure 12). The transit and occultation deviations would also have the same sign, while for apsidal precession they have opposite signs. For WASP-4, Watson & Marsh (2010) estimated that the effect could produce timing deviations of up to 15 seconds, depending on the modulation period of the stellar dynamo, and the corresponding level of differential surface shear. This cannot explain the majority our observed 78 second variation.

4.4. *Other possible explanations*

Another mechanism to produce the observed period change would be if an unseen companion in the WASP-4 system accelerated the star towards us. This would produce a period derivative

$$\dot{P} \approx \frac{\dot{v}_r P}{c}, \tag{23}$$

for $\dot{v}_r$ the time derivative of the radial velocity. Recently, Bonomo et al. (2017) collected all available HARPS data for the system, and reported no detectable slope at 3σ. However, Knutson et al. (2014) collected 5 Keck HIRES radial velocity measurements for WASP-4, and merged them with measurements from CORALIE and HARPS reported by Wilson et al. (2008), Pont et al. (2011), and Husnoo et al. (2012). Using these four datasets, Knutson et al. (2014) found that $\dot{\gamma} = -0.0099^{+0.0052}_{-0.0054}$, corresponding to a 2σ limit on the acceleration towards us of $\dot{\gamma} > -0.021\,\mathrm{m\,s^{-1}\,day^{-1}}$. This limits $\dot{P}$ to be less than 9×10^{-11} at 2σ. Our measured value is $\dot{P} = -(3.9^{+0.7}_{-0.5}) \times 10^{-10}$. We can thus rule out radial acceleration as the sole cause of the observed period change. However, it could cause up to one-quarter of the observed period decrease. Improved long-term radial velocity monitoring with the same instruments will help clarify the situation, particularly given the fact that short-term trends of roughly $\dot{\gamma} \approx 2.8\,\mathrm{m\,s^{-1}\,day^{-1}}$ are seen over timescales of order 10 days in WASP-4 (Husnoo et al. 2012). Given the known spottedness of the system (Sanchis-Ojeda et al. 2011), these short-timescale variations may also have a contribution from stellar activity.

There are two other small effects worth briefly mentioning. The first is the Shklovskii (1970) effect, in which the star's proper motion leads to a changing radial velocity. This would be apparent in the Doppler measurements described above. The effect contributes a change of order $\dot{P} \sim P\mu^2 d/c \sim 6 \times 10^{-13}$. The second effect, described by Rafikov (2009), comes from the star's on-sky motion altering our viewing angle, and leads to an observed apsidal precession. The corresponding change is $\dot{P} \sim (P\mu)^2/2\pi \sim 10^{-21}$.

Many of these phenomena are likely occurring simultaneously. From the preceding discussion, we found that radial acceleration, proper-motion, and the Applegate mechanism are unlikely to cause the timing deviations. That leaves tidal decay and apsidal precession as the possible causes.

5. FUTURE PROSPECTS
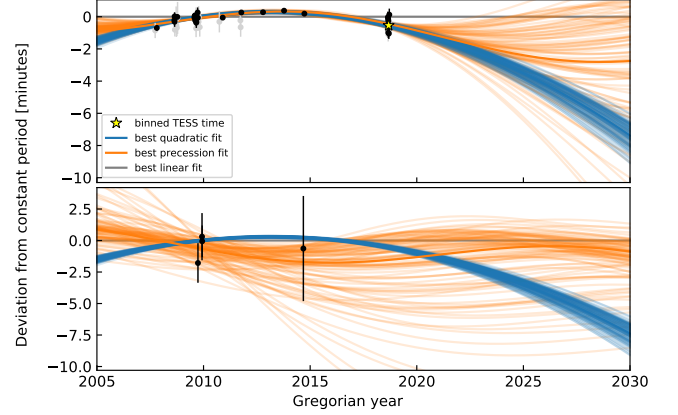
Figure 5. Future evolution possibilities for WASP-4b. Dots are as in Figure 3. Lines are 100 random samples from the posteriors of the apsidal precession model (orange), and the orbital decay model (blue). In an extended mission, TESS might re-observe WASP-4b in the early 2020s. While useful to confirm that the period is in fact changing, precise long-term monitoring past 2025 will be needed to resolve the two models.

If TESS continues observing after its primary mission, it will observe additional transits of WASP-4b in the early 2020s (Figure 5). High-precision ground-based transit measurements could also be useful. In order to rule between orbital decay and apsidal precession, occultation measurements in the near term, and also in the mid-2020s, will be helpful. Additionally, confirmation and extension of the linear trend suggested by Knutson et al. (2014) would help in understanding whether an exterior companion in the system might explain any residual eccentricity. These observations should be carried out, because they will lead to new knowledge; either a measure of the efficiency of tidal dissipation within the star, or the eccentricity and Love number of the planet. Measuring either for a single system would be rather interesting. In the coming decade, wide-field photometric surveys (TESS, HATPI, NGTS, PLATO) might even enable such measurements at a population level, which would be a good deal more interesting.

(https://www.cosmos.esa.int/gaia), processed by the *Gaia* Data Processing and Analysis Consortium (DPAC, https://www.cosmos.esa.int/web/gaia/dpac/consortium). Funding for the DPAC has been provided by national institutions, in particular the institutions participating in the *Gaia* Multilateral Agreement.

Facility: TESS (Ricker et al. 2015), Gaia (Gaia Collaboration et al. 2016, 2018)

Software: astrobase (Bhatti et al. 2018), astropy (Collaboration et al. 2018), astroquery (Ginsburg et al. 2018), BATMAN (Kreidberg 2015), corner (Foreman-Mackey 2016), emcee (Foreman-Mackey et al. 2013), IPython (Pérez & Granger 2007), matplotlib (Hunter 2007), numpy (Walt et al. 2011), pandas (McKinney 2010), scikit-learn (Pedregosa et al. 2011), scipy (Jones et al. 2001).

REFERENCES

Agol, E., Cowan, N. B., Knutson, H. A., et al. 2010, The Astrophysical Journal, 721, 1861

Anderson, D. R., Gillon, M., Hellier, C., et al. 2008, Monthly Notices of the Royal Astronomical Society, 387, L4

Anderson, D. R., Collier Cameron, A., Gillon, M., et al. 2012, Monthly Notices of the Royal Astronomical Society, 422, 1988

Applegate, J. H. 1992, The Astrophysical Journal, 385, 621

Bailey, A., & Goodman, J. 2019, Monthly Notices of the Royal Astronomical Society, 482, 1872

Baluev, R. V., Sokov, E. N., Shaidulin, V. S., et al. 2015, Monthly Notices of the Royal Astronomical Society, 450, 3101

Barnes, S. A., Weingrill, J., Fritzewski, D., Strassmeier, K. G., & Platais, I. 2016, The Astrophysical Journal, 823, 16

Batygin, K., Bodenheimer, P., & Laughlin, G. 2009, The Astrophysical Journal, 704, L49

Beerer, I. M., Knutson, H. A., Burrows, A., et al. 2011, The Astrophysical Journal, 727, 23

Belczynski, K., Kalogera, V., Rasio, F. A., et al. 2008, The Astrophysical Journal Supplement Series, 174, 223

Bhatti, W., Bouma, L. G., & Wallace, J. 2018, astrobase

Birkby, J. L., Cappetta, M., Cruz, P., et al. 2014, Monthly Notices of the Royal Astronomical Society, 440, 1470

Bonomo, A. S., Desidera, S., Benatti, S., et al. 2017, Astronomy and Astrophysics, 602, A107

Borkovits, T., Rappaport, S., Hajdu, T., & Sztakovics, J. 2015, Monthly Notices of the Royal Astronomical Society, 448, 946

Cáceres, C., Ivanov, V. D., Minniti, D., et al. 2011, Astronomy and Astrophysics, 530, A5

Campo, C. J., Harrington, J., Hardy, R. A., et al. 2011, The Astrophysical Journal, 727, 125

Carter, J. A., Yee, J. C., Eastman, J., Gaudi, B. S., & Winn, J. N. 2008, The Astrophysical Journal, 689, 499

Charbonneau, D., Allen, L. E., Megeath, S. T., et al. 2005, The Astrophysical Journal, 626, 523

Ciceri, S., Mancini, L., Southworth, J., et al. 2016, Monthly Notices of the Royal Astronomical Society, 456, 990

Claret, A. 2017, Astronomy & Astrophysics, 600, A30, arXiv: 1804.10295

Collaboration, T. A., Price-Whelan, A. M., Sipöcz, B. M., et al. 2018, arXiv:1801.02634 [astro-ph], arXiv: 1801.02634

Collier Cameron, A., & Jardine, M. 2018, Monthly Notices of the Royal Astronomical Society, 476, 2542

Counselman, C. C. 1973, The Astrophysical Journal, 180, 307

Croll, B., Lafreniere, D., Albert, L., et al. 2011, The Astronomical Journal, 141, 30

Crossfield, I. J. M., Knutson, H., Fortney, J., et al. 2012, The Astrophysical Journal, 752, 81

Dawson, R. I., & Johnson, J. A. 2018, arXiv:1801.06117 [astro-ph], arXiv: 1801.06117

Doyle, A. P., Smalley, B., Maxted, P. F. L., et al. 2013, Monthly Notices of the Royal Astronomical Society, 428, 3164

Dragomir, D., Kane, S. R., Pilyavsky, G., et al. 2011, The Astronomical Journal, 142, 115

Eastman, J., Siverd, R., & Gaudi, B. S. 2010, Publications of the Astronomical Society of the Pacific, 122, 935, arXiv: 1005.4415

Essick, R., & Weinberg, N. N. 2016, The Astrophysical Journal, 816, 18

Foreman-Mackey, D. 2016, The Journal of Open Source Software, 24

Foreman-Mackey, D., Hogg, D. W., Lang, D., & Goodman, J. 2013, Publications of the Astronomical Society of the Pacific, 125, 306

Fukui, A., Narita, N., Tristram, P. J., et al. 2011, Publications of the Astronomical Society of Japan, 63, 287

Gaia Collaboration, Prusti, T., de Bruijne, J. H. J., et al. 2016, Astronomy and Astrophysics, 595, A1

Gaia Collaboration, Brown, A. G. A., Vallenari, A., et al. 2018, Astronomy and Astrophysics, 616, A1

Geller, A. M., Hurley, J. R., & Mathieu, R. D. 2013, The Astronomical Journal, 145, 8

Gibson, N. P., Aigrain, S., Barstow, J. K., et al. 2013, Monthly Notices of the Royal Astronomical Society, 428, 3680

Gillon, M., Anderson, D. R., Triaud, A. H. M. J., et al. 2009a, Astronomy and Astrophysics, 501, 785

Gillon, M., Smalley, B., Hebb, L., et al. 2009b, Astronomy and Astrophysics, 496, 259

Giménez, A., & Bastero, M. 1995, Astrophysics and Space Science, 226, 99

Ginsburg, A., Sipocz, B., Madhura Parikh, et al. 2018, Astropy/Astroquery: V0.3.7 Release

Goldreich, P., & Soter, S. 1966, Icarus, 5, 375

Goodman, J., & Weare, J. 2010, Communications in Applied Mathematics and Computational Science, 5, 65

Hall, D. S. 1989, Space Science Reviews, 50, 219

Hansen, B. M. S. 2010, The Astrophysical Journal, 723, 285

Hebb, L., Collier-Cameron, A., Loeillet, B., et al. 2009, The Astrophysical Journal, 693, 1920

Hellier, C., Anderson, D. R., Collier Cameron, A., et al. 2009, Nature, 460, 1098

Heyl, J. S., & Gladman, B. J. 2007, Monthly Notices of the Royal Astronomical Society, 377, 1511

Hoyer, S., Rojo, P., & LÃṣpez-Morales, M. 2012, The Astrophysical Journal, 748, 22

Hoyer, S., López-Morales, M., Rojo, P., et al. 2013, Monthly Notices of the Royal Astronomical Society, 434, 46

Huitson, C. M., DÃl'sert, J.-M., Bean, J. L., et al. 2017, The Astronomical Journal, 154, 95

Hunter, J. D. 2007, Computing in Science & Engineering, 9, 90

Husnoo, N., Pont, F., Mazeh, T., et al. 2012, Monthly Notices of the Royal Astronomical Society, 422, 3151

Hut, P. 1980, Astronomy and Astrophysics, 92, 167

Ibgui, L., Burrows, A., & Spiegel, D. S. 2010, The Astrophysical Journal, 713, 751

Jackson, B., Barnes, R., & Greenberg, R. 2009, The Astrophysical Journal, 698, 1357

Jackson, B., Jensen, E., Peacock, S., Arras, P., & Penev, K. 2016, Celestial Mechanics and Dynamical Astronomy, 1

Jenkins, J. M., Twicken, J. D., McCauliff, S., et al. 2016, Software and Cyberinfrastructure for Astronomy IV, 9913, 99133E

Jones, E., Oliphant, T., Peterson, P., et al. 2001, Open source scientific tools for Python

Jordán, A., & Bakos, G. A. 2008, The Astrophysical Journal, 685, 543

Jordán, A., Espinoza, N., Rabus, M., et al. 2013, The Astrophysical Journal, 778, 184

Kass, R. E., & Raftery, A. E. 1995, Journal of the American Statistical Association, 90, 773

Knutson, H. A., Charbonneau, D., Allen, L. E., et al. 2007, Nature, 447, 183

Knutson, H. A., Fulton, B. J., Montet, B. T., et al. 2014, The Astrophysical Journal, 785, 126

Kovács, G., Zucker, S., & Mazeh, T. 2002, Astronomy and Astrophysics, 391, 369

Kozai, Y. 1962, The Astronomical Journal, 67, 591

Kreidberg, L. 2015, Publications of the Astronomical Society of the Pacific, 127, 1161

Lainey, V., Arlot, J.-E., Karatekin, Ã., & van Hoolst, T. 2009, Nature, 459, 957

Levrard, B., Winisdoerffer, C., & Chabrier, G. 2009, The Astrophysical Journal, 692, L9

Lidov, M. L. 1962, Planetary and Space Science, 9, 719

López-Morales, M., Coughlin, J. L., Sing, D. K., et al. 2010, The Astrophysical Journal, 716, L36

Maciejewski, G., Dimitrov, D., FernÃądez, M., et al. 2016, Astronomy and Astrophysics, 588, L6

MacLeod, M., Cantiello, M., & Soares-Furtado, M. 2018, The Astrophysical Journal Letters, 853, L1

Mandel, K., & Agol, E. 2002, The Astrophysical Journal, 580, L171, arXiv: astro-ph/0210099

Mansouri-Samani, M., et al. 2018, TESS Science Data Products Description Document, EXP-TESS-ARC-ICD-0014, https://archive.stsci.edu/missions/tess/doc/EXP-TESS-ARC-ICD-TM-0014.pdf

Mardling, R. A. 2007, Monthly Notices of the Royal Astronomical Society, 382, 1768

Matsakos, T., & KÃűnigl, A. 2016, The Astrophysical Journal Letters, 820, L8

Matsumura, S., Peale, S. J., & Rasio, F. A. 2010, The Astrophysical Journal, 725, 1995

Maxted, P. F. L., Anderson, D. R., Doyle, A. P., et al. 2013, Monthly Notices of the Royal Astronomical Society, 428, 2645

May, E. M., Zhao, M., Haidar, M., Rauscher, E., & Monnier, J. D. 2018, The Astronomical Journal, 156, 122

McKinney, W. 2010, in Proceedings of the 9th Python in Science Conference, ed. S. van der Walt & J. Millman, 51

Meibom, S., & Mathieu, R. D. 2005, The Astrophysical Journal, 620, 970

Metzger, B. D., Giannios, D., & Spiegel, D. S. 2012, Monthly Notices of the Royal Astronomical Society, 425, 2778

Milliman, K. E., Mathieu, R. D., Geller, A. M., et al. 2014, The Astronomical Journal, 148, 38

Moyano, M., Almeida, L. A., von Essen, C., Jablonski, F., & Pereira, M. G. 2017, Monthly Notices of the Royal Astronomical Society, 471, 650

Ni, D. 2018, Astronomy & Astrophysics, 613, A32

Nikolov, N., Henning, T., Koppenhoefer, J., et al. 2012, Astronomy and Astrophysics, 539, A159

Nikolov, N., Sing, D. K., Burrows, A. S., et al. 2015, Monthly Notices of the Royal Astronomical Society, 447, 463

Ogilvie, G. I. 2014, Annual Review of Astronomy and Astrophysics, 52, 171, arXiv: 1406.2207

Pál, A., & Kocsis, B. 2008, Monthly Notices of the Royal Astronomical Society, 389, 191

Patra, K. C., Winn, J. N., Holman, M. J., et al. 2017, The Astronomical Journal, 154, 4

Pedregosa, F., Varoquaux, G., Gramfort, A., et al. 2011, Journal of Machine Learning Research, 12, 2825

Penev, K., Bouma, L. G., Winn, J. N., & Hartman, J. D. 2018, The Astronomical Journal, 155, 165

Penev, K., Jackson, B., Spada, F., & Thom, N. 2012, The Astrophysical Journal, 751, 96

Penev, K., & Sasselov, D. 2011, The Astrophysical Journal, 731, 67

Penev, K., Hartman, J. D., Bakos, G. Ã., et al. 2016, The Astronomical Journal, 152, 127

Pérez, F., & Granger, B. E. 2007, Computing in Science and Engineering, 9, 21

Petrucci, R., Jofré, E., Ferrero, L. V., et al. 2018, Monthly Notices of the Royal Astronomical Society, 473, 5126

Petrucci, R., Jofré, E., Schwartz, M., et al. 2013, The Astrophysical Journal Letters, 779, L23

Phinney, E. S. 1992, Philosophical Transactions of the Royal Society of London Series A, 341, 39

Poddaný, S., Brát, L., & Pejcha, O. 2010, New Astronomy, 15, 297

Pont, F. 2009, Monthly Notices of the Royal Astronomical Society, 396, 1789

Pont, F., Husnoo, N., Mazeh, T., & Fabrycky, D. 2011, Monthly Notices of the Royal Astronomical Society, 414, 1278

Rafikov, R. R. 2009, The Astrophysical Journal, 700, 965

Ragozzine, D., & Wolf, A. S. 2009, The Astrophysical Journal, 698, 1778, arXiv: 0807.2856

Ranjan, S., Charbonneau, D., Désert, J.-M., et al. 2014, The Astrophysical Journal, 785, 148

Rasio, F. A., Tout, C. A., Lubow, S. H., & Livio, M. 1996, The Astrophysical Journal, 470, 1187

Ricker, G., & Vanderspek, R. 2018, Data Products From TESS Data Alerts, https://archive.stsci.edu/prepds/tess-data-alerts/index.html

Ricker, G. R., Winn, J. N., Vanderspek, R., et al. 2015, Journal of Astronomical Telescopes, Instruments, and Systems, 1, 014003

Russell, H. N. 1939, The Astrophysical Journal, 90, 641

Sada, P. V., Deming, D., Jennings, D. E., et al. 2012, Publications of the Astronomical Society of the Pacific, 124, 212

Sanchis-Ojeda, R., Winn, J. N., Holman, M. J., et al. 2011, The Astrophysical Journal, 733, 127

Schatzman, E. 1962, Annales d'Astrophysique, 25, 18

Schwarzschild, M. 1958, Structure and evolution of the stars (Princeton Univesity Press), Ch. 18

Shklovskii, I. S. 1970, Soviet Astronomy, 13, 562

Skumanich, A. 1972, The Astrophysical Journal, 171, 565

Smith, J. C., Morris, R. L., Jenkins, J. M., et al. 2017a, Kepler Science Document, 7

Smith, J. C., Stumpe, M. C., Jenkins, J. M., et al. 2017b, Kepler Science Document, 8

Söderhjelm, S. 1980, Astronomy and Astrophysics, 89, 100

Southworth, J. 2011, Monthly Notices of the Royal Astronomical Society, 417, 2166

Southworth, J., Hinse, T. C., JÃÿrgensen, U. G., et al. 2009, Monthly Notices of the Royal Astronomical Society, 396, 1023

Stassun, K. G., Oelkers, R. J., Pepper, J., et al. 2018, The Astronomical Journal, 156, 102

Sullivan, P. W., et al. 2015, ApJ, 809, 77

Thompson, S., et al. 2013, Kepler Data Release 19 Notes Q14, KSCI-19059-001, https://archive.stsci.edu/kepler/release_notes/release_notes19/DataRelease_19_20130204.pdf

Tregloan-Reed, J., Southworth, J., Burgdorf, M., et al. 2015, Monthly Notices of the Royal Astronomical Society, 450, 1760

Triaud, A. H. M. J., Collier Cameron, A., Queloz, D., et al. 2010, Astronomy and Astrophysics, 524, A25

Urban, S., & Seidelmann, P. 2012, Explanatory Supplement to the Astronomical Almanac (University Science Books)

Valsecchi, F., Rappaport, S., Rasio, F. A., Marchant, P., & Rogers, L. A. 2015, The Astrophysical Journal, 813, 101

Wahl, S. M., Hubbard, W. B., & Militzer, B. 2016, The Astrophysical Journal, 831, 14

Walt, S. v. d., Colbert, S. C., & Varoquaux, G. 2011, Computing in Science & Engineering, 13, 22

Watson, C. A., & Marsh, T. R. 2010, Monthly Notices of the Royal Astronomical Society, 405, 2037

Weinberg, N. N., Sun, M., Arras, P., & Essick, R. 2017, The Astrophysical Journal Letters, 849, L11

Wilkins, A. N., Delrez, L., Barker, A. J., et al. 2017, The Astrophysical Journal Letters, 836, L24

Williams, P. K. G., Charbonneau, D., Cooper, C. S., Showman, A. P., & Fortney, J. J. 2006, The Astrophysical Journal, 649, 1020

Wilson, D. M., Gillon, M., Hellier, C., et al. 2008, The Astrophysical Journal Letters, 675, L113

Winn, J. N. 2010, Exoplanets, 55

—. 2013, TESS Science Memo No. 1, Version 2. Available upon request.

Winn, J. N., Holman, M. J., Carter, J. A., et al. 2009, The Astronomical Journal, 137, 3826

Winn, J. N., Noyes, R. W., Holman, M. J., et al. 2005, The Astrophysical Journal, 631, 1215

Zahn, J.-P. 1977, Astronomy and Astrophysics, 500, 121

Zhou, G., Bayliss, D. D. R., Kedziora-Chudczer, L., et al. 2015, Monthly Notices of the Royal Astronomical Society, 454, 3002

Table 1. WASP-4b transit times, uncertainties, and references.

t_{tra} [BJD$_{TDB}$]	$\sigma_{t_{tra}}$ [days]	Epoch	H13?	Reference
2454368.59279	0.00033	-1059	1	Wilson et al. (2008)
2454396.69576	0.00012	-1038	1	Gillon et al. (2009b)
2454697.79817	0.00009	-813	1	Winn et al. (2009)
2454701.81280	0.00022	-810	1	Hoyer et al. (2013)
2454701.81303	0.00018	-810	1	Hoyer et al. (2013)
2454705.82715	0.00029	-807	1	Hoyer et al. (2013)
2454728.57767	0.00042	-790	1	Hoyer et al. (2013)
2454732.59197	0.00050	-787	1	Hoyer et al. (2013)
2454740.62125	0.00035	-781	1	Hoyer et al. (2013)
2454748.65111	0.00007	-775	1	Winn et al. (2009)
2454752.66576	0.00069	-772	1	Dragomir et al. (2011)
2455041.72377	0.00018	-556	1	Hoyer et al. (2013)
2455045.73853	0.00008	-553	1	Sanchis-Ojeda et al. (2011)
2455049.75325	0.00007	-550	1	Sanchis-Ojeda et al. (2011)
2455053.76774	0.00009	-547	1	Sanchis-Ojeda et al. (2011)
2455069.82661	0.00029	-535	1	Nikolov et al. (2012)
2455069.82670	0.00028	-535	1	Nikolov et al. (2012)
2455069.82617	0.00038	-535	1	Nikolov et al. (2012)
2455069.82676	0.00031	-535	1	Nikolov et al. (2012)
2455073.84128	0.00026	-532	1	Nikolov et al. (2012)
2455073.84108	0.00029	-532	1	Nikolov et al. (2012)
2455073.84111	0.00023	-532	1	Nikolov et al. (2012)
2455073.84114	0.00018	-532	1	Nikolov et al. (2012)
2455096.59148	0.00022	-515	1	Hoyer et al. (2013)
2455100.60595	0.00012	-512	1	Sanchis-Ojeda et al. (2011)
2455112.64986	0.00039	-503	1	Nikolov et al. (2012)
2455112.65009	0.00033	-503	1	Nikolov et al. (2012)
2455112.65005	0.00031	-503	1	Nikolov et al. (2012)
2455112.65005	0.00049	-503	1	Nikolov et al. (2012)
2455132.72310	0.00041	-488	1	Hoyer et al. (2013)
2455468.61943	0.00046	-237	1	Hoyer et al. (2013)
2455526.16356	0.00008	-194	0	Ranjan et al. (2014)
2455828.60375	0.00041	32	1	Hoyer et al. (2013)
2455832.61815	0.00041	35	1	Hoyer et al. (2013)
2455844.66287	0.00009	44	0	Huitson et al. (2017)
2456216.69123	0.00006	322	0	Huitson et al. (2017)
2456576.67556	0.00005	591	0	Huitson et al. (2017)
2456924.61561	0.00006	851	0	Huitson et al. (2017)
2458355.18490	0.00024	1920	0	This work
2458356.52251	0.00026	1921	0	This work
2458357.86101	0.00024	1922	0	This work
2458359.19951	0.00025	1923	0	This work
2458360.53708	0.00027	1924	0	This work
2458361.87539	0.00024	1925	0	This work
2458363.21412	0.00027	1926	0	This work
2458364.55192	0.00025	1927	0	This work
2458365.89064	0.00026	1928	0	This work
2458369.90503	0.00027	1931	0	This work
2458371.24297	0.00026	1932	0	This work
2458372.58136	0.00027	1933	0	This work
2458373.91982	0.00027	1934	0	This work
2458375.25801	0.00024	1935	0	This work

Table 1 continued

Table 1 *(continued)*

$t_{\rm tra}$ [BJD$_{\rm TDB}$]	$\sigma_{t_{\rm tra}}$ [days]	Epoch	H13?	Reference
2458376.59621	0.00024	1936	0	This work
2458377.93443	0.00026	1937	0	This work
2458379.27317	0.00026	1938	0	This work
2458380.61097	0.00027	1939	0	This work

NOTE— $t_{\rm tra}$ is the measured transit midtime, and $\sigma_{t_{\rm tra}}$ is its 1σ uncertainty. σ_{t_0} was evaluated from the sampled posteriors by taking the maximum of the difference between the 84th percentile minus the median, and the median minus the 16th percentile. The "Reference" column refers to the work describing the original observations. The "H13?" column is 1 if the mid-time value was taken from Hoyer et al. (2013). Otherwise, the mid-time came from the column listed in "Reference".

Table 2. WASP-4b occultation times, uncertainties, and references.

$t_{\rm occ}$ [BJD$_{\rm TDB}$]	$\sigma_{t_{\rm occ}}$ [days]	Epoch	Reference
2455102.61210	0.00109	-511	Cáceres et al. (2011)[a]
2455172.20159	0.00130	-459	Beerer et al. (2011)
2455174.87780	0.00087	-457	Beerer et al. (2011)
2456907.88714	0.00290	838	Zhou et al. (2015)[b]

NOTE— $t_{\rm occ}$ is the measured occultation midtime, minus the $2a/c =$ 22.8 second light travel time; $\sigma_{t_{\rm occ}}$ is the 1σ uncertainty on the occultation time.

[a] Cáceres et al. (2011) reported this time in "HJD", with an unspecified time standard. We assumed the time was originally in HJD$_{\rm UTC}$, inflated the uncertainties by 69.184 seconds, and converted to BJD$_{\rm TDB}$ for the time reported.

[b] Zhou et al. (2015) fixed the epoch, and let $e\cos\omega$ float. Using the reported dates of observation, we converted their $e\cos\omega$ values into an occultation time using Equation 1 of the text.

Table 3. Best-fit model parameters.

Parameter	Median Value (Unc.)[a]
Constant period	
t_0 [BJD$_{\rm TBD}$]	2455785.780502(+19)(-19)
P [days]	1.338231460(+22)(-22)
Constant period derivative	
t_0 [BJD$_{\rm TBD}$]	2455785.780664(+24)(-25)
P [days]	1.338231677(31)(-31)
dP/dt	$-3.83(+39)(-36) \times 10^{-10}$
Apsidal precession	
t_0 [BJD$_{\rm TBD}$]	2455785.78015(+22)(-29)
$P_{\rm s}$ [days]	1.33823131(+16)(-34)
e	$1.59^{+1.38}_{-0.64} \times 10^{-3}$
ω_0 [rad]	2.37(+35)(-30)
$d\omega/dE$ [rad epoch^{-1}]	$9.56^{+3.55}_{-2.43} \times 10^{-4}$

[a] The numbers in parenthesis give the 1σ uncertainty in the final two digits, where appropriate.

APPENDIX

A. VERIFYING THE TESS TIME STAMPS

Any systematic offset between the reported TESS times and the true barycentric reference would cast doubt on the results of this study. Such an offset would have historic precedent: Kepler had a systematic error in its timestamps that was corrected only in Q14 (Thompson et al. 2013, Section 3.4).

We devised two checks on the absolute calibration of the TESS time system. First, in § A.1, we recalculate and confirm the barycentric correction reported by SPOC in the TESS lightcurve file headers. In § A.2, we repeat the main analysis of the paper for a collection of other hot Jupiters, and use their observed transit times to rule out a global TESS time offset. The latter test confirms that WASP-4b is an outlier.

A.1. *Using the headers of the lightcurve files*

The TESS lightcurve files provide observation start and end times in three different time systems: JD_{UTC}, JD_{TDB}, and BJD_{TDB}. First, we verified for a few select lightcurve files that JD_{UTC} lagged behind JD_{TDB} by the expected $32.184 + N$ seconds, where N is the number of leap-seconds since 1961. For the relevant observation time, $N = 37$, and the offset was as expected. Then, using the JD_{UTC} timestamp, we recalculated the barycentric correction computed by SPOC, using the Eastman et al. 2010 calculator. Due to the first author's ignorance of the spacecraft's position, we performed this calculation assuming that the observer was located at the Earth's geocenter, and used the correct direction for each star. This gave us times in BJD_{TDB} that agreed with the archival times to within 1.7 seconds. This offset is comparable to the light-travel delay time expected for TESS on its orbit from perigee of $\approx 20 R_{\oplus}$ to apogee of $\approx 60 R_{\oplus}$.

This calculation bounds any error in the SPOC barycentric julian date correction to be less than 1.7 seconds. Since this is smaller than the effect of interest, we treat the BJD correction as "verified", and proceed to a subsequent test.

A.2. *Using other hot Jupiters as references*

If the observed timing delay in WASP-4b were caused by a systematic timing system offset between the TESS BJD_{TDB} times and the BJD_{TDB} reference, we would expect that it might apply to other hot Jupiters as well. This test can rule out an important class of clock error – a systematic global offset.

To rule out this possibility, we repeat the timing analysis of the main paper, for other hot Jupiters with long preceding observing baselines. We first checked which hot Jupiters were observed over the first two TESS sectors using a combination of `tessmaps`[6] and TEPCat (Southworth 2011). We then selected hot Jupiters for which there were at least five distinct epochs reported in the peer-reviewed literature. We required that each observation be of a single transit, that the midpoint be fit as a free parameter, and that the time system be clearly documented. Our final sample of hot Jupiters included WASPs-4b, -5b, -6b, -18b, and -46b. The collected and measured times are given in Tables 4, 5, 6, and 7 for each.

Using the literature timing data for each hot Jupiter, we then performed a least-squares fit to a linear ephemeris. Using the best-fit values and variances, we calculated the uncertainty on the predicted transit time during the TESS observations. This gave 9, 94, 18, 42, and 60 seconds for WASPs-4b, -5b, -6b, -18b, and -46b. If a substantial portion of the observed timing deviation in WASP-4b (about 77 seconds) were from a systematic offset in the time systems, this offset would be present in the other hot Jupiter transit times as well. We show in Figure 6 that WASP-4b is the only hot Jupiter that transited significantly earlier than expected.

To convert this intuition into a quantitative limit, for each hot Jupiter we considered the model

$$t_{\mathrm{tra}}(E) = t_0 + PE + t_{\mathrm{offset}}, \tag{A1}$$

for t_{offset} a systematic constant offset between the reported timestamps and the true BJD_{TDB} reference. Our priors were

$$t_0 \sim \mathcal{N}[t_0', \sigma_{t_0'}], \tag{A2}$$

$$P \sim \mathcal{N}[P', \sigma_{P'}], \tag{A3}$$

$$t_{\mathrm{offset}} \sim \mathcal{U}[-20\sigma_{t_0'}, 20\sigma_{t_0'}], \tag{A4}$$

where $\mathcal{N}$ and $\mathcal{U}$ denote a normal and uniform distribution, (t_0', P') are the best-fit reference time and period using only the literature transit times, and $(\sigma_{t_0'}, \sigma_{P'})$ are their uncertainties.

For each planet, we then ask: what fraction of the posterior for t_{offset} is consistent with an offset worse than 77 seconds? For WASP-4b, the answer is unsurpringly about half. For WASP-6b, the most constraining object, about 1 sample in 2 million is

---

[6] github.com/lgbouma/tessmaps
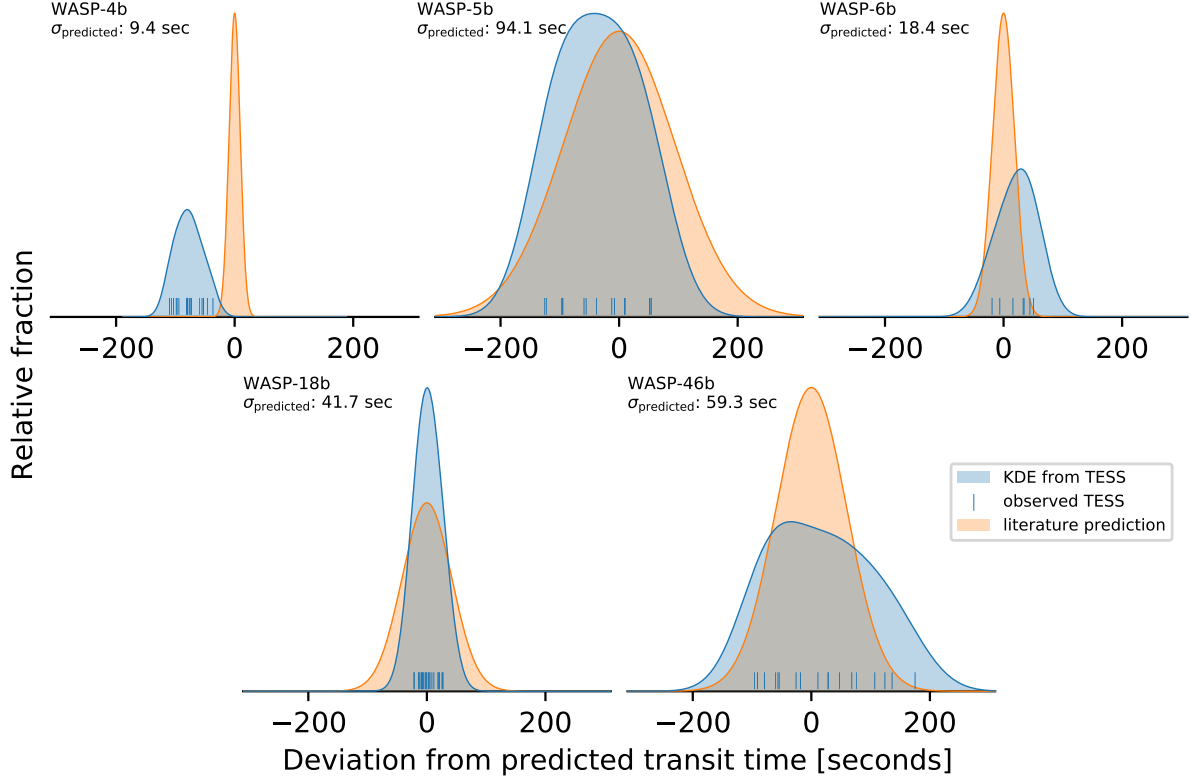
Figure 6. There is no evidence for a systematic offset between TESS times and the barycentric reference. While the WASP-4b transits fell about 75 seconds earlier than predicted, other well-observed hot Jupiters, in particular WASP-6b and WASP-18b, arrived on time. Ticks are observed TESS transit midtimes; the blue distribution function is a kernel density estimate; the orange distribution function is a gaussian centered on zero using the indicated 1σ standard deviation in the prediction ($\sigma_{\mathrm{predicted}}$).

consistent with such a timing offset (4.9σ). For WASP-18b, 1 in 63 samples would be consistent with this timing offset (2.1σ), and in WASP-46b, the limit is 1 in 38 samples (1.9σ). For WASP-5b, the predicted time is too imprecise to rule out timing offsets at the necessary amplitude. Multiplying the three independent probabilities for WASPs-5b, 6b, and -18b, we rule out $t_{\mathrm{offset}} < -77$ seconds at 6.3σ, or about about 1 part in 5 billion.

Table 4. WASP-5b transit times, uncertainties, and references.

t_{tra} [BJD$_{\mathrm{TDB}}$]	$\sigma_{t_{\mathrm{tra}}}$ [days]	Epoch	Reference
2454383.76750	0.00040	-885	Anderson et al. (2008)
2454387.02275	0.00100	-883	Anderson et al. (2008)
2454636.17459	0.00082	-730	Fukui et al. (2011)
2454699.68303	0.00041	-691	Hoyer et al. (2012)
2454707.82465	0.00052	-686	Hoyer et al. (2012)
2454707.82523	0.00025	-686	Southworth et al. (2009)
2454730.62243	0.00031	-672	Southworth et al. (2009)
2454730.62301	0.00076	-672	Hoyer et al. (2012)
2454761.56356	0.00047	-653	Hoyer et al. (2012)
2454772.96212	0.00075	-646	Fukui et al. (2011)
2454774.59093	0.00030	-645	Hoyer et al. (2012)
2454787.61792	0.00069	-637	Hoyer et al. (2012)
2455005.82714	0.00036	-503	Hoyer et al. (2012)

Table 4 continued

BOUMA ET AL.

Table 4 *(continued)*

t_{tra} [BJD$_{TDB}$]	$\sigma_{t_{tra}}$ [days]	Epoch	Reference
2455049.79540	0.00080	-476	Hoyer et al. (2012)
2455075.84947	0.00056	-460	Dragomir et al. (2011)
2455079.10830	0.00079	-458	Fukui et al. (2011)
2455110.04607	0.00089	-439	Fukui et al. (2011)
2455123.07611	0.00079	-431	Fukui et al. (2011)
2455129.58759	0.00043	-427	Hoyer et al. (2012)
2455364.08150	0.00110	-283	Fukui et al. (2011)
2455377.10955	0.00093	-275	Fukui et al. (2011)
2455448.75927	0.00110	-231	Dragomir et al. (2011)
2456150.61479	0.00056	200	Moyano et al. (2017)
2456150.61396	0.00057	200	Moyano et al. (2017)
2458355.50829	0.00083	1554	This work
2458357.13741	0.00071	1555	This work
2458358.76412	0.00068	1556	This work
2458360.39377	0.00070	1557	This work
2458362.02273	0.00073	1558	This work
2458363.64908	0.00090	1559	This work
2458365.27827	0.00071	1560	This work
2458366.90627	0.00075	1561	This work
2458370.16411	0.00076	1563	This work
2458371.79126	0.00071	1564	This work
2458373.42123	0.00075	1565	This work
2458375.04910	0.00069	1566	This work
2458376.67856	0.00074	1567	This work
2458378.30530	0.00087	1568	This work
2458379.93419	0.00082	1569	This work

NOTE— t_{tra} is the measured transit midtime, and $\sigma_{t_{tra}}$ is its 1σ uncertainty. The "Reference" column refers to the work describing the original observations. All the literature times except for the two Moyano et al. (2017) times are from the homogeneous Hoyer et al. (2012) analysis.

Table 5. WASP-6b transit times, uncertainties, and references.

t_{tra} [BJD$_{TDB}$]	$\sigma_{t_{tra}}$ [days]	Epoch	Reference
2454425.02167	0.00022	-398	Gillon et al. (2009a)
2455009.83622	0.00021	-224	Tregloan-Reed et al. (2015)
2455046.80720	0.00015	-213	Tregloan-Reed et al. (2015)
2455073.69529	0.00013	-205	Tregloan-Reed et al. (2015)
2455409.79541	0.00010	-105	Tregloan-Reed et al. (2015)
2455446.76621	0.00058	-94	Dragomir et al. (2011)
2455473.65439	0.00097	-86	Jordán et al. (2013)
2455846.72540	0.00045	25	Sada et al. (2012)
2456088.71801	0.00013	97	Nikolov et al. (2015)
2456095.43974	0.00017	99	Nikolov et al. (2015)
2456132.41082	0.00017	110	Nikolov et al. (2015)
2458357.39410	0.00033	772	This work
2458360.75573	0.00033	773	This work
2458364.11691	0.00032	774	This work
2458370.83872	0.00033	776	This work
2458374.19952	0.00031	777	This work

Table 5 continued

Table 5 *(continued)*

t_{tra} [BJD$_{TDB}$]	$\sigma_{t_{tra}}$ [days]	Epoch	Reference
2458377.56026	0.00033	778	This work
2458380.92185	0.00038	779	This work

NOTE— t_{tra} is the measured transit midtime, and $\sigma_{t_{tra}}$ is its 1σ uncertainty. The "Reference" column refers to the work describing the original observations.

Table 6. WASP-18b transit times, uncertainties, and references.

t_{tra} [BJD$_{TDB}$]	$\sigma_{t_{tra}}$ [days]	Epoch	Reference
2454221.48163	0.00038	-3730	Hellier et al. (2009)
2455221.30420	0.00010	-2668	Maxted et al. (2013)
2455432.18970	0.00010	-2444	Maxted et al. (2013)
2455470.78850	0.00040	-2403	Maxted et al. (2013)
2455473.61440	0.00090	-2400	Maxted et al. (2013)
2455554.57860	0.00050	-2314	Maxted et al. (2013)
2455570.58400	0.00048	-2297	Maxted et al. (2013)
2455876.55590	0.00130	-1972	Maxted et al. (2013)

Table 6 continued

Table 6 *(continued)*

t_{tra} [BJD$_{TDB}$]	$\sigma_{t_{tra}}$ [days]	Epoch	Reference
2456896.14780	0.00080	-889	Wilkins et al. (2017)
2457255.78320	0.00030	-507	Wilkins et al. (2017)
2457319.80100	0.00039	-439	Wilkins et al. (2017)
2458354.45778	0.00015	660	This work
2458355.39934	0.00015	661	This work
2458356.34073	0.00016	662	This work
2458357.28228	0.00017	663	This work
2458358.22348	0.00017	664	This work
2458359.16512	0.00016	665	This work
2458360.10662	0.00016	666	This work
2458361.04813	0.00017	667	This work
2458361.98968	0.00016	668	This work
2458362.93129	0.00016	669	This work
2458363.87266	0.00018	670	This work
2458364.81373	0.00016	671	This work
2458365.75526	0.00017	672	This work
2458366.69704	0.00019	673	This work
2458367.63835	0.00187	674	This work
2458369.52126	0.00017	676	This work
2458370.46285	0.00017	677	This work
2458371.40405	0.00016	678	This work
2458372.34536	0.00017	679	This work
2458373.28727	0.00017	680	This work
2458374.22817	0.00016	681	This work
2458375.16976	0.00016	682	This work
2458376.11124	0.00017	683	This work
2458377.05269	0.00016	684	This work
2458377.99448	0.00017	685	This work
2458378.93572	0.00016	686	This work
2458379.87720	0.00016	687	This work
2458380.81891	0.00017	688	This work

NOTE— t_{tra} is the measured transit midtime, and $\sigma_{t_{tra}}$ is its 1σ uncertainty. The "Reference" column refers to the work describing the original observations. All the literature times are from the homogeneous Wilkins et al. (2017) analysis.

Table 7. WASP-46b transit times, uncertainties, and references.

t_{tra} [BJD$_{TDB}$]	$\sigma_{t_{tra}}$ [days]	Epoch	Reference
2455396.60785	0.00062	-673	Anderson et al. (2012)
2455449.53082	0.00026	-636	Anderson et al. (2012)
2455722.73178	0.00023	-445	Ciceri et al. (2016)
2455757.06195	0.00094	-421	Petrucci et al. (2018)
2455858.61833	0.00009	-350	Ciceri et al. (2016)
2456108.92771	0.00094	-175	Petrucci et al. (2018)
2456111.79422	0.00016	-173	Ciceri et al. (2016)
2456111.79413	0.00012	-173	Ciceri et al. (2016)
2456111.79424	0.00015	-173	Ciceri et al. (2016)
2456130.38895	0.00042	-160	Petrucci et al. (2018)
2456131.81456	0.00112	-159	Petrucci et al. (2018)
2456194.75916	0.00027	-115	Ciceri et al. (2016)

Table 7 continued

Table 7 *(continued)*

t_{tra} [BJD$_{TDB}$]	$\sigma_{t_{tra}}$ [days]	Epoch	Reference
2456217.64127	0.00015	-99	Ciceri et al. (2016)
2456217.64156	0.00013	-99	Ciceri et al. (2016)
2456227.65574	0.00060	-92	Petrucci et al. (2018)
2456407.88096	0.00015	34	Ciceri et al. (2016)
2456407.88085	0.00018	34	Ciceri et al. (2016)
2456407.88148	0.00028	34	Ciceri et al. (2016)
2456407.88159	0.00043	34	Ciceri et al. (2016)
2456460.80526	0.00017	71	Ciceri et al. (2016)
2456460.80450	0.00024	71	Ciceri et al. (2016)
2456460.80547	0.00064	71	Ciceri et al. (2016)
2456510.86818	0.00060	106	Petrucci et al. (2018)
2456510.86699	0.00015	106	Petrucci et al. (2018)
2456516.58667	0.00119	110	Petrucci et al. (2018)
2456520.88012	0.00064	113	Petrucci et al. (2018)
2456533.75260	0.00071	122	Ciceri et al. (2016)
2456533.75480	0.00015	122	Ciceri et al. (2016)
2456576.66289	0.00109	152	Petrucci et al. (2018)
2456589.54197	0.00090	161	Petrucci et al. (2018)
2456609.56653	0.00043	175	Petrucci et al. (2018)
2456839.85440	0.00123	336	Petrucci et al. (2018)
2456862.74085	0.00048	352	Petrucci et al. (2018)
2456882.76566	0.00073	366	Petrucci et al. (2018)
2456885.62429	0.00053	368	Petrucci et al. (2018)
2456915.66040	0.00123	389	Petrucci et al. (2018)
2456942.83880	0.00078	408	Petrucci et al. (2018)
2456948.56384	0.00074	412	Petrucci et al. (2018)
2457274.68458	0.00184	640	Petrucci et al. (2018)
2457294.70886	0.00140	654	Petrucci et al. (2018)
2457550.74797	0.00031	833	Petrucci et al. (2018)
2457593.65692	0.00024	863	Petrucci et al. (2018)
2457600.80985	0.00039	868	Petrucci et al. (2018)
2457610.82286	0.00020	875	Petrucci et al. (2018)
2458326.00972	0.00091	1375	This work
2458327.43899	0.00093	1376	This work
2458328.86970	0.00094	1377	This work
2458330.29965	0.00105	1378	This work
2458331.73234	0.00105	1379	This work
2458333.15977	0.00086	1380	This work
2458334.59230	0.00095	1381	This work
2458336.02222	0.00082	1382	This work
2458337.45111	0.00099	1383	This work
2458340.31143	0.00093	1385	This work
2458341.74347	0.00093	1386	This work
2458343.17362	0.00093	1387	This work
2458344.60303	0.00110	1388	This work
2458346.03436	0.00091	1389	This work
2458347.46335	0.00168	1390	This work
2458348.89621	0.00086	1391	This work
2458350.32672	0.00101	1392	This work
2458351.75486	0.00103	1393	This work

NOTE— t_{tra} is the measured transit midtime, and $\sigma_{t_{tra}}$ is its 1σ uncertainty. The "Reference" column refers to the work describing the original observations. All the literature times are from the homogeneous Petrucci et al. (2018) analysis. 14 of the lightcurves were acquired by ETD observers (see Petrucci et al. 2018).